Received: 26 June 2020 | Revised: 17 August 2020 | Accepted: 18 August 2020

DOI: 10.1002/jcc.26412

FULL PAPER

Journal of COMPUTATIONAL CHEMISTRY WILEY

Real-time time-dependent density functional theory using density fitting and the continuous fast multipole method

Carolin Müller | Manas Sharma | Marek Sierka

Otto Schott Institute of Materials Research, Friedrich Schiller University of Jena, Jena, Germany

Correspondence
Marek Sierka, Otto Schott Institute of Materials Research, Friedrich Schiller University of Jena, Löbdergraben 32, 07743 Jena, Germany.
Email: marek.sierka@uni-jena.de

Funding information
Deutsche Forschungsgemeinschaft, Grant/Award Number: Projekt number 398816777 - SFB 1375 (project A04)

Abstract

An implementation of real-time time-dependent density functional theory (RT-TDDFT) within the TURBOMOLE program package is reported using Gaussian-type orbitals as basis functions, second and fourth order Magnus propagator, and the self-consistent field as well as the predictor–corrector time integration schemes. The Coulomb contribution to the Kohn–Sham matrix is calculated combining density fitting approximation and the continuous fast multipole method. Performance of the implementation is benchmarked for molecular systems with different sizes and dimensionalities. For linear alkane chains, the wall time for density matrix time propagation step is comparable to the Kohn-Sham (KS) matrix construction. However, for larger two- and three-dimensional molecules, with up to about 5,000 basis functions, the computational effort of RT-TDDFT calculations is dominated by the KS matrix evaluation. In addition, the maximum time step is evaluated using a set of small molecules of different polarities. The photoabsorption spectra of several molecular systems calculated using RT-TDDFT are compared to those obtained using linear response time-dependent density functional theory and coupled cluster methods.

KEYWORDS

continuous fast multipole method, density fitting, density functional theory, electron dynamics, real-time real-space TDDFT

1 | INTRODUCTION

Time-dependent density functional theory (TDDFT) is a reasonable compromise between accuracy and moderate computational cost for investigations of response properties and dynamics of molecules and extended systems in the presence of time-dependent fields. In the weak excitation limit the linear-response TDDFT (LR-TDDFT), which extracts excitation frequencies of the system as poles of the density response function, is usually sufficient.[1,2] However, fundamental understanding of nonlinear excited state dynamics at the femto- and sub-femtosecond time scale requires going beyond the linear response. The strong excitation regime and sub-femtosecond excitation time are best captured with a real-time, real-space TDDFT (RT-TDDFT). It allows to directly monitor the time evolution of electron density (e.g., see References [3-6]), which gives the opportunity to shed light on fundamental mechanisms of excitation processes. Furthermore, LR-TDDFT requires the solution of an eigenvalue equation for a matrix written in the space of electron–hole pairs, which scales as $\mathcal{O}(N^6)$. In practice, this scaling can be improved to $\mathcal{O}\left(N^3\right)$ through efficient implementation and methods employing the Liouville-Lanczos approach.[7] In contrast, RT-TDDFT scales in the range of $\mathcal{O}\left(N^2\right)$ to $\mathcal{O}\left(N^3\right)$ and is, therefore, an efficient alternative to LR-TDDFT for large systems. Additionally, fully nonlinear spectral information across broad spectral regions in large systems can be

readily obtained.[4,8] RT-TDDFT offers many promising applications for the understanding of basic physical processes such as light harvesting, photodissociation, electron transport, higher harmonic emission, charge transfer dynamics, molecular conductivity and spin dynamics, to name a few.[6,9] Due to its increasing popularity, RT-TDDFT has been implemented in several software packages like GAUSSIAN, NWCHEM, OCTOPUS, QBOX, Q-CHEM, SIESTA, etc.[4,7,8,10–22]

One of the limitations of RT-TDDFT is that the exchange correlation part of the Kohn-Sham (KS) matrix is generally non-local in both space and time. It is also formally a functional of the initial wave function and the entire history of the density.[23] It has been shown that the neglect of these "memory effects" (i.e., locality in time) within the adiabatic approximation is valid not only in the linear response range of excitation fields but also has an exact high-frequency strong-field limit.[24] For fields with an intermediate frequency and strength, it appears that the adiabatic approximation can lead to large errors. In particular, when densities of the ground and excited states differ significantly, since current state-of-the-art density functional approximations are derived for the ground state.[25] However, the errors are usually more pronounced for smaller systems and decrease with the system size. This has been attributed to the decreasing difference between the ground and excited states densities for larger systems.[3] Nevertheless, the accuracy of RT-TDDFT simulations must, in most of the cases, be assessed by a comparison with measured spectroscopic observables or results of accurate wave-function-based quantum mechanical calculations.

In this work, an efficient RT-TDDFT implementation within the TURBOMOLE program package[26,27] using density fitting and continuous fast multipole method (DF-CFMM)[28] is presented. The efficiency and the scaling performance of different parts of the program are analyzed. Various benchmarks using two different propagation schemes are presented, probing the factors affecting the accuracy and computational performance of RT-TDDFT.

2 | THEORY

This section summarizes the main equations and approximations used in our implementation. More detailed information can be found in References [4, 12].

2.1 | Real-time time dependent density functional theory

In RT-TDDFT, the time evolution of electron density $\rho(\mathbf{r}, t)$ is monitored directly by solving the set of effective one particle time-dependent Kohn–Sham (KS) equations

$$\mathrm{i}\frac{\partial \psi_m(\mathbf{r},t)}{\partial t} = \left[-\frac{1}{2}\nabla^2 + v_{\mathrm{eff}}[\rho](\mathbf{r},t)\right]\psi_m(\mathbf{r},t), \tag{1}$$

where $v_{\mathrm{eff}}[\rho](\mathbf{r},t)$ is an effective potential uniquely described by $\rho(\mathbf{r}, t)$[29] that contains all nuclear-electron v_{ne}, exchange-correlation $v_{\mathrm{xc}}[\rho]$, electronic Coulomb $v_J[\rho]$ and external field v_E potentials. The electron density is obtained as a sum over N_{MO} KS molecular orbitals (MO) $\psi_m(\mathbf{r}, t)$ with occupation numbers f_m

$$\rho(\mathbf{r},t) = \sum_{m=1}^{N_{\mathrm{MO}}} f_m |\psi_m(\mathbf{r},t)|^2. \tag{2}$$

In practical applications, $\psi_m(\mathbf{r}, t)$ are expanded in a set of N_{bf} basis functions $\mu(\mathbf{r})$

$$\psi_m(\mathbf{r},t) = \sum_{\mu=1}^{N_{\mathrm{bf}}} C_{\mu m}(t)\mu(\mathbf{r}), \tag{3}$$

with $C_{\mu m}(t)$ as elements of the time-dependent molecular orbital coefficient matrix $\mathbf{C}(t)$. For molecular systems, Gaussian-type orbitals (GTO) are commonly used basis functions, offering both computational efficiency and flexibility. In RT-TDDFT employing GTO basis, the time evolution of $\rho(\mathbf{r}, t)$, represented by the single particle reduced density matrix $\mathbf{D}(t)$ with elements

$$D_{\mu\nu}(t) = \sum_{m=1}^{N_{\mathrm{MO}}} f_m C^{\dagger}_{\mu m}(t) C_{\nu m}(t), \tag{4}$$

is governed by the von Neumann equation

$$\mathrm{i}\frac{\partial \mathbf{D}(t)}{\partial t} = [\mathbf{F}(t), \mathbf{D}(t)], \tag{5}$$

where $\mathbf{F}(t)$ is the time-dependent KS matrix in the orthonormal basis of MO. $\mathbf{F}(t)$ is obtained from the KS matrix in the (non-orthonormal) GTO basis using simple transformation involving eigenvectors and eigenvalues of the GTO overlap matrix $\mathbf{S}$ (cf. Section 3.1).[4,30]

The most efficient methods for numerical integration of the von Neumann equation, Equation (5), are based on the Magnus expansion,[31,32] which uses a unitary propagator $\mathcal{U}(t+\Delta t, t) = e^{\mathbf{\Omega}_1 + \mathbf{\Omega}_2 + \mathbf{\Omega}_3 + \cdots}$ that conserves the idempotency of $\mathbf{D}(t)$

$$\mathbf{D}(t+\Delta t) = \mathcal{U}(t+\Delta t, t)\mathbf{D}(t)\mathcal{U}^{\dagger}(t+\Delta t, t). \tag{6}$$

Applying Gauss–Legendre quadrature[33] to evaluate $\mathbf{\Omega}_1$ and $\mathbf{\Omega}_2$ the resulting expressions are

$$\mathbf{\Omega}_1(t+\Delta t, t) \approx -\mathrm{i}\cdot\Delta t\cdot\mathbf{F}\left(t+\frac{\Delta t}{2}\right) \text{ and} \tag{7}$$

$$\mathbf{\Omega}_2(t+\Delta t, t) \approx \frac{\sqrt{3}\Delta t^2}{12}\left[\mathbf{F}\left(t+\frac{3-\sqrt{3}}{6}\Delta t\right), \mathbf{F}\left(t+\frac{3+\sqrt{3}}{6}\Delta t\right)\right]. \tag{8}$$

This approximation is valid to order Δt^{2p}, where p is the number of terms in the exponential expansion of $\mathcal{U}(t+\Delta t,t)$ (here p is 1 or 2).[4,31]

2.2 | Electric field

The electric field **E** is assumed to be uniform over the whole molecule, that is, **E**(**r**, t) = **E**(t). This electric dipole approximation has the advantage that the electric field contribution to the KS matrix **F** is an additive term

$$\mathbf{F} = \mathbf{F}^0 + \mathbf{F}^E, \tag{9}$$

where $\mathbf{F}^0$ is the KS matrix of the unperturbed system. $\mathbf{F}^E$ is the perturbation matrix

$$\mathbf{F}^E_{\mu\nu} = -\sum_{j=x,y,z} M^j_{\mu\nu} E_j, \quad j = x,y,z \tag{10}$$

with the electric field vector (E_x, E_y, E_z) and the dipole moment matrices $\mathbf{M}^j$

$$M^j_{\mu\nu} = -\int \mu(\mathbf{r})\, j\nu(\mathbf{r})\, d\mathbf{r}. \tag{11}$$

Since the electric field is considered to be uniform over the whole molecule, the electric dipole approximation is only valid for wavelengths much larger than the size of the molecule, that is, $\mathbf{k}\cdot\mathbf{r} \equiv \frac{2\pi}{\lambda}\cdot(\mathbf{r}_{max}-\mathbf{r}_0) \approx 0$, where $\mathbf{r}_0$ is the center of the molecule, $\mathbf{r}_{max}$ is the coordinate of the atom farthest from the center and $\mathbf{k} = \frac{2\pi}{\lambda}$ is the wavenumber and λ the wavelength of the electric field.

2.3 | Absorption spectra

Absorption spectra can be calculated using the following expression for the dipole strength function[4]

$$S(\omega) = \frac{1}{3}\cdot\frac{4\pi\omega}{c} Tr\left(\mathrm{Im}\left[\alpha_{ij}\right]\right), \quad i,j = x,y,z \tag{12}$$

where α_{ij} is the complex polarizability tensor, related to the induced dipole moment $\mu_j^{ind}(\omega)$ and the external electric field vector **E** in the frequency space by

$$\mu_j^{ind}(\omega) = \alpha_{ij}(\omega) E_i(\omega). \tag{13}$$

α_{ij} can be obtained using the Fourier transforms of **E** and $\mu_j^{ind}(\omega)$ as

$$\alpha_{ij}(\omega) = \frac{\int_{-\infty}^{\infty} e^{i\omega t}\mu_j^{ind}(t) e^{-\gamma t} dt}{\int_{-\infty}^{\infty} e^{i\omega t} E_i(t) dt}, \tag{14}$$

with the damping factor γ (typically in the range of 0.003–0.005 au = 124–207 ps^{-1}).[12]

The time-dependent induced dipole moment is defined as

$$\mu_j^{ind}(t) = \mu_j(t) - \mu_j^0, \tag{15}$$

where μ_j^0 is the dipole moment of the unperturbed system and

$$\mu_j(t) = Tr\left[\mathbf{M}^j \cdot \mathbf{D}(t)\right], \quad j = x,y,z. \tag{16}$$

$\mathbf{M}^j$ are the dipole moment matrices, Equation (11), and **D** is the density matrix, Equation (4). In this work, the absorption spectrum was calculated using a Gaussian electric field pulse

$$E_i(t) = A e^{-\frac{(t-t_0)^2}{2w^2}}, \tag{17}$$

where A is the amplitude, t_0 is the center of the pulse and w is the half-width of the pulse.

Electron density plots were obtained by exciting the system using a laser pulse of the form

$$E_i(t) = A e^{-\frac{(t-t_0)^2}{2w^2}} \cos(\omega_0 t), \tag{18}$$

where ω_0 is the pulse frequency.

3 | IMPLEMENTATION DETAILS

3.1 | Time evolution operator

The time evolution operator for the second order Magnus expansion is implemented as

$$\mathcal{U}(\Delta t, 0) = e^{-i\cdot\Delta t\cdot\mathbf{F}\left(\frac{\Delta t}{2}\right)}, \tag{19}$$

with **F** in the orthonormal MO basis.[31] **F** is obtained transforming $\mathbf{F}_{AO}$ expressed in an non-orthonormal atomic orbital (AO) basis,[4]

$$\mathbf{F} = \mathbf{X}^T \mathbf{F}_{AO} \mathbf{X}, \quad \mathbf{X} = \mathbf{U}\mathbf{s}^{-1/2}, \tag{20}$$

where **U** is the eigenvector matrix of the overlap matrix **S**, and **s** is a diagonal matrix containing eigenvalues of **S**. Density matrix is transformed between the AO ($\mathbf{D}_{AO}$) to MO (**D**) bases as[4]

$$\mathbf{D}_{AO} = \mathbf{X}^{T}\mathbf{D}\mathbf{X}, \quad \mathbf{D} = s\mathbf{X}^{T}\mathbf{D}_{AO}\mathbf{X}s. \tag{21}$$

The exponential in Equation (19) is calculated employing diagonalization of **F** since the efficiency and parallel performance of diagonalization algorithms has significantly improved in the recent years.[34–37] Other techniques like polynomial expansions, splitting schemes, Lanczos, Padé approximation, etc.[10,38–40] are also frequently employed for the calculation of the exponential. Reference [10] compares the performance of Lanczos method with fourth order Taylor and Chebyshev expansions. One should note that for plane wave or grid-based methods, diagonalization may not be very desirable due to the large sizes of matrices. Using diagonal representation of **F** Equation (19) can be written as

$$\mathcal{U}(\Delta t,0) = \mathbf{V}\mathbf{z}(\mathbf{V}\mathbf{z})^{T} = \mathbf{A}\mathbf{A}^{T}, \tag{22}$$

where **V** is the eigenvector matrix of **F** and **z** is a diagonal matrix with elements

$$z_i = \sqrt{e^{-\mathbb{i}\cdot\Delta t\cdot\lambda_i}} \tag{23}$$

calculated using eigenvalues λ_i of **F**. Expressing $\mathcal{U}(\Delta t,0)$ as $\mathbf{A}\mathbf{A}^{T}$ reduces computational cost by almost half compared to full general matrix–matrix multiplication by leveraging specialized ZSYRK routine within BLAS.[41]

The fourth order term of the Magnus expansion of the time evolution operator is calculated as

$$\mathcal{U}(\Delta t,0) = e^{\frac{\sqrt{3}\Delta t^2}{12}[\mathbf{F}(t_1),\mathbf{F}(t_2)]}. \tag{24}$$

Since the commutator in the exponent is built of two symmetric KS matrices, the resulting matrix is skew-symmetric, which when multiplied by $\mathbb{i}$ yields a Hermitian matrix. Therefore, the calculation can be sped up by re-writing Equation (24) as

$$\mathcal{U}(\Delta t,0) = \mathbf{V}e^{-\frac{\sqrt{3}\Delta t^2}{12}\mathbb{i}\cdot\boldsymbol{\lambda}}\mathbf{V}^{\dagger} = \mathbf{V}\mathbf{z}\mathbf{V}^{\dagger}, \tag{25}$$

with

$$z_i = e^{-\frac{\sqrt{3}\Delta t^2}{12}\mathbb{i}\cdot\lambda_i}, \tag{26}$$

where $-\mathbb{i}\lambda_i$ are the eigenvalues of the original commutator matrix $[\mathbf{F}(t_1),\mathbf{F}(t_2)]$.

3.2 | Density matrix propagation

The time propagation of the density matrix using Equation (6) is calculated in an orthonormal MO basis. This implementation differs from others[4,7,10–13,15,17,42–45] by building up the time evolution operator with every step instead of the density matrix. For example, propagation from time $t = 0$ to $2\Delta t$ is achieved through the following steps.

$$\text{Step 1}: \mathbf{D}(\Delta t) = \mathcal{U}(\Delta t,0)\mathbf{D}(0)\mathcal{U}^{\dagger}(\Delta t,0) \tag{27}$$

$$\text{Step 2}: \mathbf{D}(2\Delta t) = \mathcal{U}^{\dagger}(2\Delta t,0)\mathbf{D}(0)\mathcal{U}^{\dagger}(2\Delta t,0) \tag{28}$$

where $\mathcal{U}(2\Delta t,0) = \mathcal{U}(2\Delta t,\Delta t)\mathcal{U}(\Delta t,0)$.

In addition to the step-wise building of the time evolution operator, the initial density matrix is split as

$$\mathbf{D}(0) = \mathbf{C}(0)\sqrt{\mathbf{f}}\cdot\left[\mathbf{C}(0)\sqrt{\mathbf{f}}\right]^{\dagger} = \mathbf{C}^{0}\mathbf{C}^{0^{\dagger}}, \tag{29}$$

where **C** and **f** denote the orbitals coefficient matrix and the diagonal occupation number matrix, respectively. This allows to perform the density matrix time propagation step using two matrix–matrix multiplications

$$\mathcal{U}(t+\Delta t,0)\cdot\mathbf{C}^{0} = \mathbf{M} \tag{30}$$

and

$$\mathbf{D}(t+\Delta t) = \mathbf{M}\mathbf{M}^{\dagger}. \tag{31}$$

The advantage of using Equations (30) and (31) are the reduced $N_{bf} \times N_{occ}$ dimensions of **M**, where N_{bf} and N_{occ} are the number of basis functions and occupied orbitals, respectively, with $N_{occ} \ll N_{bf}$ in most cases. This significantly speeds up the density matrix time propagation step compared to using the full $N_{bf} \times N_{bf}$ matrices. In addition, using $\mathbf{M}\mathbf{M}^{\dagger}$ in Equation (31) reduces computational cost by almost half compared to full general matrix–matrix multiplication. Furthermore, since $\mathbf{D}(t + \Delta t)$ is a real symmetric matrix, only the real part of $\mathbf{M}\mathbf{M}^{\dagger}$ needs to be calculated by leveraging specialized DSYRK routine within BLAS.[41]

3.3 | Time integration methods

Two time integration methods were implemented, the self-consistent field (SCF) procedure and the predictor–corrector (PC) scheme.[15] For simplicity, both integration methods are described here only for the second order Magnus expansion.

3.3.1 | SCF procedure

The procedure is initiated with the ground state density $\mathbf{D}(0)$ and KS $\mathbf{F}(0)$ matrices, respectively. In the first step $\mathbf{F}(0)$ is used as a guess for $\mathbf{F}(\frac{1}{2}\Delta t)$, which is improved upon iteratively, until the density matrix $\mathbf{D}(\Delta t)$ is converged. The algorithm can be summarized as follows:

1. Initial guess: $\mathbf{F}(\frac{1}{2}\Delta t) \approx \mathbf{F}(0)$
2. Build time evolution operator: $\mathcal{U}(\Delta t,0) = e^{-i\cdot\Delta t\cdot\mathbf{F}(\frac{1}{2}\Delta t)}$
3. Calculate: $\mathbf{D}^i(\Delta t) = \mathcal{U}(\Delta t,0)\mathbf{D}(0)\mathcal{U}^\dagger(\Delta t,0)$ (i denotes SCF step)
4. Convergence test: $[\mathbf{D}^{i-1}(\Delta t) - \mathbf{D}^i(\Delta t)]^2 \le \epsilon_{crit}$, if converged, go to (7)
5. Calculate $\mathbf{F}(\Delta t)$ from $\mathbf{D}^i(\Delta t)$ and from the electric field information $\mathbf{E}(\Delta t)$
6. Linear interpolation: $\mathbf{F}(\frac{1}{2}\Delta t) = \frac{1}{2}[\mathbf{F}(0) + \mathbf{F}(\Delta t)]$, continue with (2)
7. Linear extrapolation: $\mathbf{F}(1\frac{1}{2}\Delta t) = 1\frac{1}{2}\mathbf{F}(\Delta t) + \frac{1}{2}\mathbf{F}(0)$
8. Build time evolution operator for the second time step: $\mathcal{U}(2\Delta t,0) = \mathcal{U}(2\Delta t,\Delta t)\cdot\mathcal{U}(\Delta t,0) = e^{-i\cdot\Delta t\cdot\mathbf{F}(1\frac{1}{2}\Delta t)}\cdot\mathcal{U}(\Delta t,0)$
9. Propagate density matrix: $\mathbf{D}^i(2\Delta t) = \mathcal{U}(2\Delta t,0)\mathbf{D}(0)\mathcal{U}^\dagger(2\Delta t,0)$

...

A closely resembling SCF procedure using second order Magnus expansion has been implemented in Reference [46].

3.3.2 | Predictor–corrector scheme

In the PC scheme, the initial KS matrices $\mathbf{F}(t - \frac{1}{2}\Delta t)$ and $\mathbf{F}(t - 1\frac{1}{2}\Delta t)$ have to be calculated with the SCF procedure described above. The PC procedure includes the following steps

1. Linear extrapolation: $\mathbf{F}(t + \frac{1}{4}\Delta t) = 1\frac{3}{4}\mathbf{F}(t - \frac{1}{2}\Delta t) - \frac{3}{4}\mathbf{F}(t - 1\frac{1}{2}\Delta t)$
2. Build time evolution operator: $\mathcal{U}(t+\frac{1}{2}\Delta t,0) = \mathcal{U}(t+\frac{1}{2}\Delta t,t)\cdot\mathcal{U}(t,0) = e^{-i\cdot\frac{1}{2}\Delta t\cdot\mathbf{F}(t+\frac{1}{4}\Delta t)}\cdot\mathcal{U}(t,0)$
3. Propagate density matrix: $\mathbf{D}(t+\frac{1}{2}\Delta t) = \mathcal{U}(t+\frac{1}{2}\Delta t,0)\mathbf{D}(0)\mathcal{U}^\dagger(t+\frac{1}{2}\Delta t,0)$
4. Calculate $\mathbf{F}(t + \frac{1}{2}\Delta t)$ from $\mathbf{D}(t + \frac{1}{2}\Delta t)$ and from the electric field information $\mathbf{E}(t + \frac{1}{2}\Delta t)$
5. Build time evolution operator: $\mathcal{U}(t+\Delta t,0) = \mathcal{U}(t+\Delta t,t)\cdot\mathcal{U}(t,0) = e^{-i\cdot\Delta t\cdot\mathbf{F}(t+\frac{1}{2}\Delta t)}\cdot\mathcal{U}(t,0)$
6. Propagate density matrix: $\mathbf{D}(t+\Delta t) = \mathcal{U}(t+\Delta t,0)\mathbf{D}(0)\mathcal{U}^\dagger(t+\Delta t,0)$

...

A similar scheme has also been implemented in NWCHEM by Lopata and co-workers.[4] As an alternative to the linear extrapolation scheme described above, an exponential PC scheme has also been suggested recently.[16] Another popular technique for time integration uses the modified midpoint unitary transformation (MMUT) approach which preserves the time reversal symmetry.[17] In contrast to the above schemes (SCF and PC), MMUT requires only one Fock matrix construction per time step. However, it only allows for very small time steps.[16] Furthermore, the above schemes, allow to check on-the-fly for divergence of the propagation which is not the case for MMUT.[16]

3.4 | Methods and basis sets

All DFT calculations employ the Perdew–Burke–Ernzerhof (PBE) exchange-correlation functional.[47] The performance and scaling behavior of the RT-TDDFT implementation is investigated using the split-valence plus polarization (SVP) basis sets.[48,49] Evaluations of the Coulomb term use the combined density fitting and continuous fast multipole method (DF-CFMM)[28] along with corresponding auxiliary basis sets.[50] Coupled cluster (CC2) calculations used valence triple-zeta basis set with two sets of polarization functions (def2-TZVPP)[49] with 48 frozen lowest occupied orbitals.

The calculations are performed on the 2.2 GHz Intel Xeon E7-8890 v4 CPU. Parallel efficiency is evaluated using up to 32 CPU cores. Unless stated otherwise, RT-TDDFT calculations are performed using the PC scheme, 2nd order Magnus expansion, 0.5 au time step size and a propagation time of 1,000 au (≈24 fs). A Gaussian pulse with an amplitude of $A = 2\times10^{-5}$au = 10 mV/nm, a width of w = 0.2 au = 4.8 as and t_0 = 3 au = 73 as is used for excitations [cf. Equation (17)]. UV-spectra calculation use γ = 0.004 au =165 ps^{-1} [cf. Equation (14)]. The density matrix convergence criterion in the ground state SCF procedure is set to 10^{-8}.

3.5 | Benchmark systems

The performance and scaling behavior of the implementation is evaluated for different sets of molecular systems with examples shown in Figure 1. They are similar to those used by Sodt et al.[51] and consist of (a) alkane chains, (b) H-terminated graphene sheets, and (c) H-terminated diamond clusters. The alkane chains have the composition C_nH_{2n+2}, with n = 10, 20, 40, 60, 160, and 200 and the longest chain uses 5,010 GTO basis and 17,024 auxiliary basis functions. The graphene sheets, $C_{16}H_{10}$, $C_{76}H_{22}$, $C_{102}H_{26}$, $C_{184}H_{34}$, $C_{210}H_{38}$, and

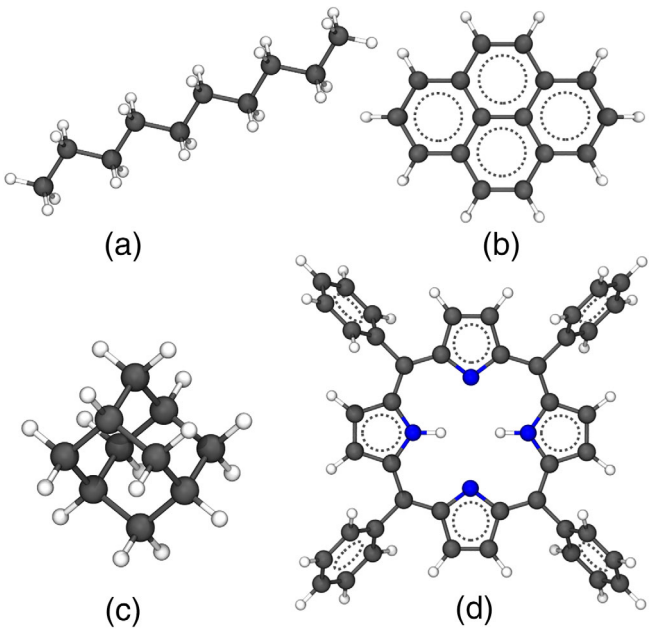

FIGURE 1 Examples of benchmark molecular systems: (a) alkane chain, (b) H-terminated graphene sheet, (c) H-terminated diamond cluster, (d) tetraphenylporphyrin [Color figure can be viewed at wileyonlinelibrary.com]

$C_{294}H_{42}$, contain up to 4,620 basis and 18,438 auxiliary basis functions. The diamond clusters have compositions $C_{11}H_{18}$, $C_{87}H_{64}$, $C_{168}H_{130}$, and $C_{246}H_{184}$. The largest cluster uses 4,610 basis and 17,214 auxiliary basis functions.

Benchmarks of the time integration accuracy and RT-TDDFT excitation energies use H_2, HF, H_2O, CO, CH_4, and C_6H_6 molecules, with the corresponding number of GTO basis functions 10, 20, 25, 30, 35, and 120, respectively. In addition, benchmark RT-TDDFT calculations were performed for tetraphenylporphyrin (TPP) shown in Figure 1.

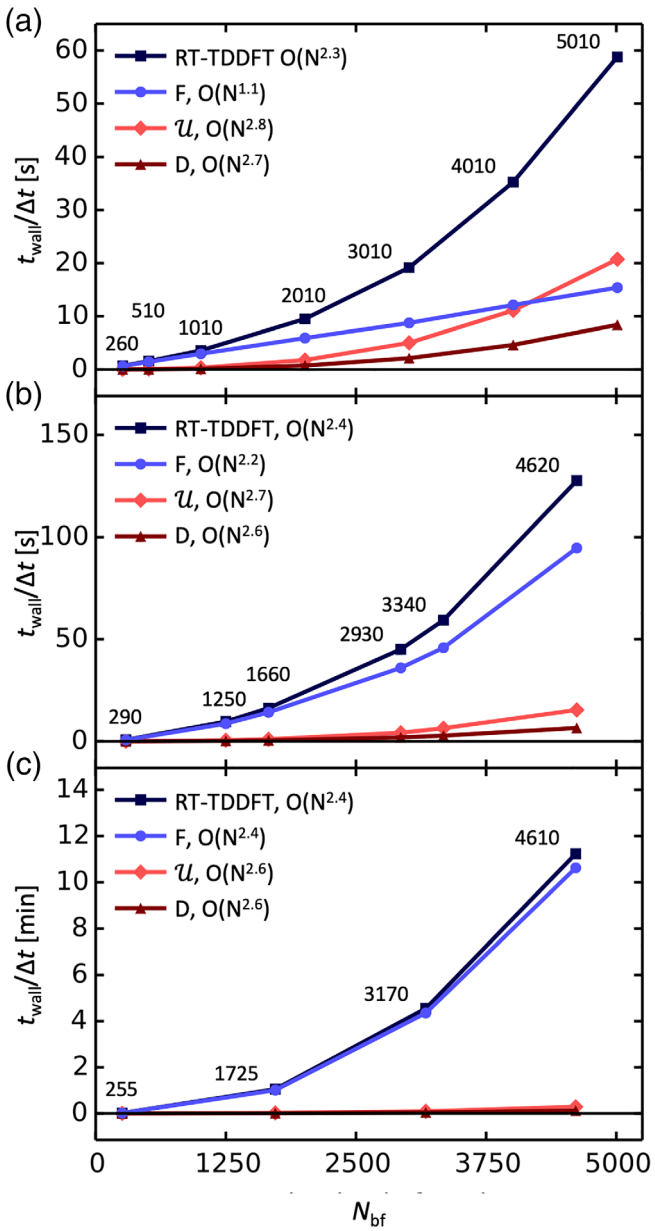

FIGURE 2 Wall time per time step $t_{wall}/\Delta t$ as a function of the number of Cartesian basis functions N_{bf} of a RT-TDDFT calculation investigated for (a) alkane chains, (b) graphene sheets, and (c) diamond clusters of different size: total RT-TDDFT step; construction of KS matrix F; construction of time evolution operator $\mathcal{U}$; density matrix propagation step D [Color figure can be viewed at wileyonlinelibrary.com]

4 | PERFORMANCE AND ACCURACY

4.1 | Timings

The wall times for the total RT-TDDFT step, KS matrix and time evolution operator ($\mathcal{U}$) construction (Equation (19)), and propagation of the density matrix (Equation (6)) using 4 CPU cores are shown in Figure 2. For the alkane chains, the wall time for calculation of the time evolution operator ($\mathcal{U}$) and the density matrix propagation is comparable to the KS matrix construction. However, for graphene sheets and diamond cluster the impact of $\mathcal{U}$ and **D** calculation is almost negligible. This is because, in contrast to the KS matrix formations, the wall time for the construction of $\mathcal{U}$ is independent of the molecular structure. Figure 2 demonstrates that except for the alkanes, the bottleneck is formation of the KS matrix. The fitted scaling exponent for the total RT-TDDFT step is 2.3 for alkane chains and 2.4 for graphene sheets and diamond clusters. The scaling exponents for the less expensive $\mathcal{U}$ and **D** calculations are approximately 2.6–2.8 and 2.6–2.7, respectively, for all the systems. To check the dependency of the scaling behavior on number of processors, we also calculate the scaling exponents of various steps for alkane chains using 16 and 32 CPU cores. The results are summarized in Table 1. The scaling exponents for KS matrix remain practically the same (≈1.1), while the exponents for **D** and $\mathcal{U}$ calculations show a reasonable decrease from 2.7 to 2.2 and from 2.8 to 2.5 respectively, when going from 4 to 32 CPU cores. However, the scaling exponent of the total RT-TDDFT step is practically unaffected by the increase in number of CPU cores. We would also like to note here, that in Reference [39], it was found that the scaling behavior of diagonalization with respect to Chebyshev expansion method becomes unfavorable with increasing number of CPU cores. We, however, observe that, looking at the diagonalization step (a key component of $\mathcal{U}$ calculation) alone, such a behavior is not apparent. To gain a better understanding, we also provide the timings and parallel efficiencies of the various steps for the largest alkane chain (5,010 GTO basis functions) in Table 2. It is observed that the KS matrix exhibits the highest parallel efficiency amongst all the steps. The parallel efficiency of $\mathcal{U}$ and **D** calculation decreases from 59% to 34%, and 52% to 31% respectively when going from 16 to 32 CPU cores. While the $\mathcal{U}$ calculation consists of a matrix–matrix multiplication as well as a matrix diagonalization, the **D** calculation only consists of matrix multiplications. This shows that diagonalization is not any more inefficiently parallelized than matrix multiplication. Therefore, we expect the implementation to perform as well as those employing splitting schemes like Baker-Campbell-Hausdorff (BCH) for the calculation of matrix exponential.[4,46] Evidently, the $\mathcal{U}$ calculation took between 35% to 42% and **D** calculation took 14–19% of the total RT-TDDFT step. This is in line with the observations reported by de la Lande and co-workers,[46] where the matrix multiplications involved in BCH approximation and transformation of the density and KS matrices between AO and MO basis were the most dominant part of the calculation taking up more than 44% of the simulation time.

4.2 | Time step and small molecules

In addition to the timings, the influence of the time step on the accuracy of the spectral information was examined for small molecules of varying polarity: H_2, HF, CO, CH_4, H_2O, and C_6H_6. The accuracy was deemed sufficient based on the following criteria: (1) the excitation energies are within 0.2 *e*V, and (2) all intensities are within 10% of the reference LR-TDDFT values. Since the maximum time step is also a function of the frequency range that has been taken into account, a constant range up to 32 *e*V was chosen. Table 3 shows the resulting maximal possible time step.

The average maximum time step is 15 as, which corresponds to 23% of the theoretical maximum time step ($\Delta t_{theo} = \pi/\omega_{max} = \pi/32$ *e*V ≈ 65 as). This shows that choosing time steps up to 20% of the theoretical maximum should be a safe choice to achieve reliable results. The average maximum time step Δt_{max} for low-polarity molecules (H_2, CH_4, C_6H_6) of 17 (18) as is slightly larger than for highly polar molecules (HF, CO) of 13 (15) as. A closer look at the average values with respect to the method, reveals that the PC scheme with 2nd order Magnus expansion performs slightly better (Δt_{max} = 16 as) than the others, and SCF method with 4th order Magnus expansion a little worse (Δt_{max} = 14 as) for the density matrix convergence criterion of 10^{-6}. However, tightening the convergence criterion to 10^{-8} improves the time step size for SCF calculations (2nd and 4th order Magnus expansion to Δt_{max} = 19 and 17 as, respectively). This improvement comes with the self-consistent character of the SCF method, for which increased number of cycles can stabilize the calculation whereas PC always performs one cycle per time step no matter which convergence criterion is chosen.

However, using a bigger time step does not automatically result in a faster calculation, since in SCF, more cycles per time step are performed for larger time steps. Figure 3 shows the wall time to propagate the electron density for 1 fs normalized to 1 basis function (s/(fs · bf)). Hereby, the systems are evolved for 24.2 fs (= 1,000 au) in total. It shows that, although the time step of SCF is greater for the 10^{-8} convergence criterion (cf. Table 3), which should result in a faster calculation (since less steps are needed to propagate the density for 24.2 fs), it results in an increased wall time (Figure 3, M2/SCF8, M4/SCF8). The best performance for all test molecules is achieved with the 2nd order Magnus expansion with PC scheme and 10^{-6} convergence criterion. Good performance is also achieved using 4th order Magnus expansion with PC and 2nd order Magnus expansion with SCF.

Finally, Figure 4 shows the photoabsorption spectrum of benzene calculated with RT-TDDFT and LR-TDDFT. It is evident that the RT-TDDFT absorption spectrum is in excellent agreement with the LR-TDDFT one. This is expected as in the weak perturbation limit RT-TDDFT and LR-TDDFT results should be equivalent. We would also like to note here, that the accuracy of the RT-TDDFT results depends critically on the size of the basis set and exchange correlation approximation employed for the calculation. Table 4 shows the comparison of lowest excitation energies of various small molecules obtained using experiments, LR-TDDFT and RT-TDDFT with different basis sets. It can be seen that the excitation energy of Benzene greatly improves from 7.16 eV using def2-SVP (Figure 4) to 6.86 eV when using a larger def2-TZVPPD[49] basis set. This is in excellent agreement with the measured value of 6.90 eV.[4] Furthermore, the error is within 10% of the measured value for all the molecules for def2-TZVPPD basis set. While this shows the effect of the size of basis set on the results, for a detailed comparison of the accuracy of different exchange-correlation functionals and coupled cluster

TABLE 1 Scaling exponents of total RT-TDDFT step; construction of KS matrix F; construction of time evolution operator $\mathcal{U}$ and density matrix propagation step D, for alkane chains with different number of CPU cores

	CPU cores		
Step	**4**	**16**	**32**
RT-TDDFT	2.3	2.3	2.2
F	1.1	1.1	1.2
$\mathcal{U}$	2.8	2.7	2.5
D	2.7	2.4	2.2

TABLE 2 Alkane chain (602 atoms, 5,010 basis functions): Wall times (s) per time step and parallel efficiency $E_{\%}$ for total RT-TDDFT step; construction of KS matrix F; construction of time evolution operator $\mathcal{U}$; density matrix propagation step D

CPU	RT-TDDFT		*F*		$\mathcal{U}$		D	
cores	*t* (s)	$E_{\%}$	*t* (s)	$E_{\%}$	*t* (s)	$E_{\%}$	*t* (s)	$E_{\%}$
4	58.78		15.38		20.73		8.39	
16	22.79	65	5.02	76	8.84	59	4.06	52
32	17.82	41	3.44	56	7.52	34	3.42	31

TABLE 3 Maximum time step [as] needed to reproduce LR-TDDFT spectra up to 32 *e*V for small molecules using the SCF and PC methods. M2 and M4 denote 2nd and 4th order Magnus expansion, respectively

	H_2		CH_4		C_6H_6		HF		CO		H_2O		Average	
	SCF	PC	SCF	PC	SCF	PC	SCF	PC	SCF	PC	SCF	PC	SCF	PC
M2	13 (15)	15	16 (19)	19	17 (21)	21	17 (21)	14	11 (16)	11	14 (21)	16	15 (19)	16
M4	11 (12)	19	16 (16)	16	22 (22)	17	14 (17)	13	12 (21)	9	12 (13)	16	14 (17)	15

Note: Density matrix convergence criterion for SCF 10^{-6}, values in brackets correspond to 10^{-8}.

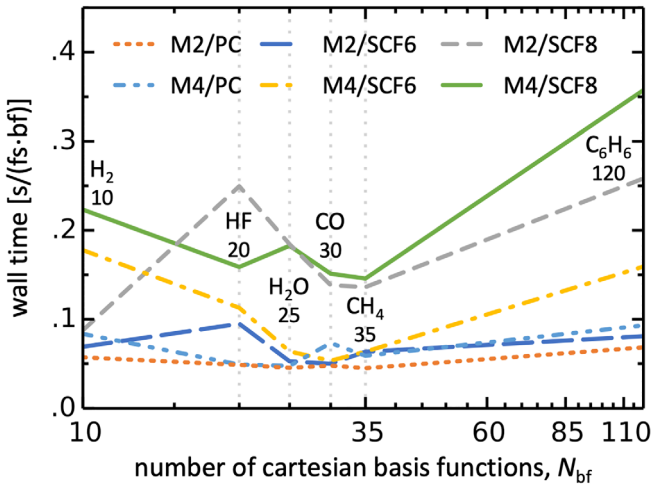

FIGURE 3 Wall time [s] per basis function to propagate the electron density for 1 fs for H_2, HF, CO, CH_4, H_2O, and C_6H_6 molecules. The maximum time step from Table 3 was chosen. M, Magnus; 2/4, 2nd/4th order; PC, predictor corrector scheme; SCF, self-consistent field method; 6/8, convergence criterion of $10^{-6/8}$ [Color figure can be viewed at wileyonlinelibrary.com]

methods in the calculation of excitation energies we refer the reader to References [52, 53].

4.3 | Excitation spectra of larger systems

Tetraphenylporphyrin (TPP) was used to test the accuracy of our RT-TDDFT implementation for larger systems. The calculated photoabsorption spectra were compared to LR-TDDFT,[4] experiment,[55] and CC2 method. Figure 5 shows the comparison of spectra normalized to the same height.

The agreement between RT-TDDFT and LR-TDDFT results is very good for the whole spectral range, up to the ionization energy (≈6 *e*V). The inset in Figure 5 shows the low energy range from ≈1.8 to 2.5 *e*V and compares the RT-TDDFT result with CC2 and experiment.[55] The experimental spectrum shows four low energy peaks (at 1.91, 2.1, 2.26, 2.41 *e*V), whereas calculated spectra give only two peaks (CC2 at 2.0, 2.26 *e*V; LR and RT at 1.92, 2.04 *e*V). The origin of these four experimental features has been extensively discussed, starting with the four-orbital model introduced

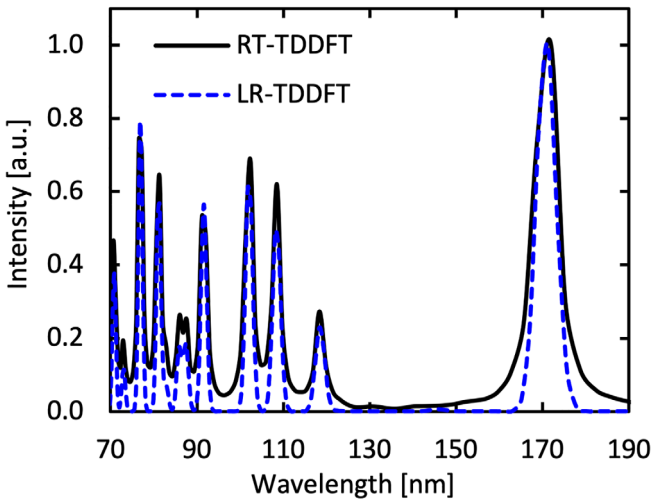

FIGURE 4 RT-TDDFT and LR-TDDFT photoabsorption spectrum of C_6H_6. LR-TDDFT spectrum is convoluted using a Gaussian line shape function with a half-width of 0.1 *e*V [Color figure can be viewed at wileyonlinelibrary.com]

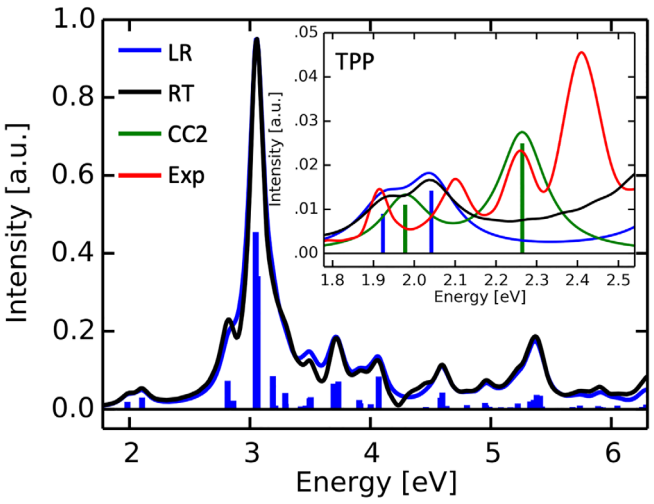

FIGURE 5 Photoabsorption spectra of TPP calculated with RT-TDDFT (RT), LR-TDDFT (LR), CC2 method, and measured experimentally (Exp).[55] LR and CC2 roots are Lorentzian broadened with full width at half maximum of .15 *e*V [Color figure can be viewed at wileyonlinelibrary.com]

TABLE 4 Lowest excitation energies (*e*V) obtained from experiments, LR-TDDFT and RT-TDDFT using def2-SVP and def2-TZVPPD basis sets with PBE exchange-correlation functional

Basis set	Method	H_2	CH_4	C_6H_6	CO	H_2O
def2-SVP	RT-TDDFT	13.19	11.07	7.16	8.33	7.21
	LR-TDDFT	13.20	11.07	7.18	8.33	7.21
def2-TZVPPD	RT-TDDFT	11.86	9.52	6.86	8.25	6.66
	LR-TDDFT	11.87	9.51	6.81	8.23	6.66
	Expt.[4,54]	11.19	9.70	6.90	8.55	7.40

by Gouterman.[56] The four peaks are described as so-called Q band with $Q_x(0–0)$, $Q_x(0–1)$, $Q_y(0–0)$ and $Q_y(0–1)$ excitations, going from low to high energies. All Q band excitations result from forbidden transitions. However, due to molecular vibrations the forbidden transitions became weakly allowed resulting in the low intensity Q bands. The $Q_x(0–1)$ and $Q_y(0–1)$ excitations were also attributed to the Frank–Condon and Herzberg–Teller effects by Minaev et al.[57]

5 | SUMMARY

This work describes an RT-TDDFT implementation within the TURBOMOLE program package, which employs Gaussian-type orbitals as basis functions along with second and fourth order Magnus expansions. Time integration uses the self-consistent field as well as the predictor–corrector schemes. The Coulomb contribution to the Kohn–Sham matrix is calculated combining density fitting approximation and the continuous fast multipole method. Performance of the implementation is benchmarked for molecular systems with different sizes and dimensionalities. For linear alkane chains, the wall time for density matrix time propagation step is comparable to the Kohn-Sham (KS) matrix construction.

However, for larger two- and three-dimensional molecules the most demanding step is the calculation of the KS matrix. In case of diamond cluster with 5,010 basis functions it accounts for 95% of the whole RT-TDDFT calculation wall time. In contrast, the generation of the time evolution operator including diagonalization of the KS matrix requires only 2.5% of the total wall time.

In addition, the average maximum time step of 15 as was found for proper reproduction of photoabsorption spectra (up to 32 *e*V) using a set of small molecules of different polarity. The choice of the time integration scheme (SCF and PC) or the order of Magnus (M2 and M4) expansion has little effect on the maximum time step. The polarity of a molecule has a greater influence, where the maximum time step of 17 as can be taken for nonpolar molecules. Considering the total RT-TDDFT wall time M2/PC performs best, followed by M2/SCF and M4/PC.

In all tested cases the photoabsorption spectra calculated using RT-TDDFT showed excellent agreement with those obtained using linear response TDDFT.

ACKNOWLEDGMENTS

Authors gratefully acknowledge financial support from the Turbomole GmbH. This work was further supported by the German Research foundation DFG (CRC 1375 NOA) project A4. Open access funding enabled and organized by Projekt DEAL.

ORCID

Manas Sharma https://orcid.org/0000-0002-5346-6280

Marek Sierka https://orcid.org/0000-0001-8153-3682

REFERENCES

[1] M. E. CASIDA. In Recent Advances in Density Functional Methods, Part 1; D. P. Chong, Ed.; World Scientific, Singapore, 1995, p.155.
[2] M. E. Casida, *Recent Developments and Applications of Modern Density Functional Theory*, (Eds: J. M. Seminario) Elsevier, Amsterdam **1996**, p. 391.
[3] S. A. Fischer, C. J. Cramer, N. Govind, *J. Chem. Theory Comput.* **2015**, *11*, 4294.
[4] K. Lopata, N. Govind, *J. Chem. Theory Comput.* **2011**, *7*, 1344.
[5] W. Ma, Y. Jiao, S. Meng, *Phys. Chem. Chem. Phys.* **2013**, *15*, 17187.
[6] J. J. Goings, P. J. Lestrange, X. Li, *Wiley Interdiscip. Rev. Comput. Mol. Sci.* **2018**, *8*, e1341.
[7] C. O'Rourke, D. R. Bowler, *J. Chem. Phys.* **2015**, *143*, 102801.
[8] Y. Takimoto, F. D. Vila, J. J. Rehr, *J. Chem. Phys.* **2007**, *127*, 154114.
[9] M. R. Provorse, C. M. Isborn, *Int. J. Quantum Chem.* **2016**, *116*, 739.
[10] A. Castro, M. A. Marques, A. Rubio, *J. Chem. Phys.* **2004**, *121*, 3425.
[11] J. Jakowski, K. Morokuma, *J. Chem. Phys.* **2009**, *130*, 224106.
[12] U. N. Morzan, F. F. Ramirez, M. B. Oviedo, C. G. Sanchez, D. A. Scherlis, M. C. Lebrero, *J. Chem. Phys.* **2014**, *140*, 164105.
[13] J. Sun, J. Song, Y. Zhao, W. Z. Liang, *J. Chem. Phys.* **2007**, *127*, 234107.
[14] W. Jia, D. An, L. W. Wang, L. Lin, *J. Chem. Theory Comput.* **2018**, *14*, 5645.
[15] C.-L. Cheng, J. S. Evans, T. Van Voorhis, *Phys. Rev. B* **2006**, *74*, 155112.
[16] Y. Zhu, J. M. Herbert, *J. Chem. Phys.* **2018**, *148*, 044117.
[17] X. Li, S. M. Smith, A. N. Markevitch, D. A. Romanov, R. J. Levis, H. B. Schlegel, *Phys. Chem. Chem. Phys.* **2005**, *7*, 233.
[18] X. Andrade, D. Strubbe, U. De Giovannini, A. H. Larsen, M. J. T. Oliveira, J. Alberdi-Rodriguez, A. Varas, I. Theophilou, N. Helbig, M. J. Verstraete, L. Stella, F. Nogueira, A. Aspuru-Guzik, A. Castro, M. A. L. Marques, A. Rubio, *Phys. Chem. Chem. Phys.* **2015**, *17*, 31371.
[19] A. Schleife, E. W. Draeger, Y. Kanai, A. A. Correa, *J. Chem. Phys.* **2012**, *137*, 22A546.
[20] W. Liang, C. T. Chapman, X. Li, *J. Chem. Phys.* **2011**, *134*, 184102.
[21] T. S. Nguyen, J. Parkhill, *J. Chem. Theory Comput.* **2015**, *11*, 2918.
[22] G. Donati, A. Wildman, S. Caprasecca, D. B. Lingerfelt, F. Lipparini, B. Mennucci, X. Li, *J. Phys. Chem. Lett.* **2017**, *8*, 5283.
[23] N. T. Maitra, K. Burke, C. Woodward, *Phys. Rev. Lett.* **2002**, *89*, 023002.
[24] R. Baer, *J. Mol. Struct.: THEOCHEM* **2009**, *914*, 19.
[25] N. T. Maitra, *J. Chem. Phys.* **2016**, *144*, 220901.
[26] TURBOMOLE developer version, a development of the University of Karlsruhe and Forschungszentrum Karlsruhe GmbH, 1989-2007, and TURBOMOLE GmbH, since 2007. http://www.turbomole.com.
[27] R. Ahlrichs, M. Bär, M. Häser, H. Horn, C. Kölmel, *Chem. Phys. Lett.* **1989**, *162*, 165.
[28] R. Łazarski, A. M. Burow, M. Sierka, *J. Chem. Theory Comput.* **2015**, *11*, 3029.
[29] E. Runge, E. K. U. Gross, *Phys. Rev. Lett.* **1984**, *52*, 997.
[30] A. Szabo, N. Ostlund, *Modern Quantum Chemistry*, Dover Publications, Mineola, NY **1996**.
[31] S. Blanes, F. Casas, J. A. Oteo, J. Ros, *Phys. Rep.* **2009**, *470*, 151.
[32] W. Magnus, *Commun. Pure Appl. Math.* **1954**, *7*, 649.
[33] A. Iserles, S. P. Nørsett, *Philos. Trans. R. Soc. Lond. A* **1999**, *357*, 983.
[34] A. Haidar, J. Kurzak, P. Luszczek. in *Proc. Int. Conf. on High Performance Computing, Networking, Storage and Analysis*, ACM, Denver, Colorado, **2013**, p 1.
[35] A. Haidar, H. Ltaief, J. Dongarra, *SIAM J. Sci. Comput.* **2012**, *34*, C249.
[36] A. Haidar, H. Ltaief, J. Dongarra, in *Proc. 2011 Int. Conf. for High Performance Computing, Networking, Storage and Analysis*, ACM, Seattle, Washington, **2011**, p. 1.
[37] F. Tisseur, J. Dongarra, *SIAM J. Sci. Comput.* **1999**, *20*, 2223.
[38] C. Moler, C. Van Loan, *SIAM Rev.* **2003**, *45*, 3.

[39] D. Williams-Young, J. J. Goings, X. Li, *J. Chem. Theory Comput.* **2016**, *12*, 5333.
[40] M. Arioli, B. Codenotti, C. Fassino, *Linear Algebra Appl.* **1996**, *240*, 111.
[41] L. S. Blackford, J. Demmel, J. Dongarra, I. Duff, S. Hammarling, G. Henry, M. Heroux, L. Kaufman, A. Lumsdaine, A. Petitet, R. Pozo, K. Remington, R. C. Whaley, *ACM Trans. Math. Softw.* **2002**, *28*, 135.
[42] F. Ding, B. E. Van Kuiken, B. E. Eichinger, X. Li, *J. Chem. Phys.* **2013**, *138*, 064104.
[43] C. M. Isborn, X. Li, *J. Chem. Phys.* **2008**, *129*, 204107.
[44] X. Li, J. C. Tully, H. B. Schlegel, M. J. Frisch, *J. Chem. Phys.* **2005**, *123*, 084106.
[45] M. R. Provorse, B. F. Habenicht, C. M. Isborn, *J. Chem. Theory Comput.* **2015**, *11*, 4791.
[46] X. Wu, J.-M. Teuler, F. Cailliez, C. Clavaguéra, D. R. Salahub, A. de la Lande, *J. Chem. Theory Comput.* **2017**, *13*, 3985.
[47] J. P. Perdew, K. Burke, M. Ernzerhof, *Phys. Rev. Lett.* **1996**, *77*, 3865.
[48] A. Schäfer, H. Horn, R. Ahlrichs, *J. Chem. Phys.* **1992**, *97*, 2571.
[49] F. Weigend, R. Ahlrichs, *Phys. Chem. Chem. Phys.* **2005**, *7*, 3297.
[50] F. Weigend, *Phys. Chem. Chem. Phys.* **2006**, *8*, 1057.
[51] A. Sodt, J. E. Subotnik, M. Head-Gordon, *J. Chem. Phys.* **2006**, *125*, 194109.
[52] S. Tussupbayev, N. Govind, K. Lopata, C. J. Cramer, *J. Chem. Theory Comput.* **2015**, *11*, 1102.
[53] K. Lopata, R. Reslan, M. Kowalska, D. Neuhauser, N. Govind, K. Kowalski, *J. Chem. Theory Comput.* **2011**, *7*, 3686.
[54] P. Verma, Y. Wang, S. Ghosh, X. He, D. G. Truhlar, *J. Phys. Chem. A* **2019**, *123*, 2966.
[55] M. Lan, H. Zhao, H. Yuan, C. Jiang, S. Zuo, Y. Jiang, *Dyes Pigm.* **2007**, *74*, 357.
[56] M. Gouterman, *J. Mol. Spectrosc.* **1961**, *6*, 138.
[57] B. Minaev, Y. H. Wang, C. K. Wang, Y. Luo, H. Agren, *Spectrochim. Acta A Mol. Biomol. Spectrosc.* **2006**, *65*, 308.

How to cite this article: Müller C, Sharma M, Sierka M. Real-time time-dependent density functional theory using density fitting and the continuous fast multipole method. *J Comput Chem*. 2020;41:2573–2582. https://doi.org/10.1002/jcc.26412